Chaotic mixing in three-dimensional microvascular networks fabricated by direct-write assembly

DANIEL THERRIAULT[1], SCOTT R. WHITE*[2,3] AND JENNIFER A. LEWIS*[3,4]

[1]Department of Aerospace Engineering, [2]Departments of Aerospace Engineering and Theoretical and Applied Mechanics, [3]Beckman Institute, [4]Departments of Material Science and Engineering and Chemical Engineering, and Frederick Seitz Materials Research Laboratory, University of Illinois at Urbana-Champaign, Urbana, Illinois 61801, USA
*e-mail: swhite@uiuc.edu; jalewis@uiuc.edu

Published online: 23 March 2003; doi:10.1038/nmat863

The creation of geometrically complex fluidic devices is a subject of broad fundamental and technological interest. Here, we demonstrate the fabrication of three-dimensional (3D) microvascular networks through direct-write assembly of a fugitive organic ink. This approach yields a pervasive network of smooth cylindrical channels (~10–300 μm) with defined connectivity. Square-spiral towers, isolated within this vascular network, promote fluid mixing through chaotic advection. These vertical towers give rise to dramatic improvements in mixing relative to simple straight (1D) and square-wave (2D) channels while significantly reducing the device planar footprint. We envisage that 3D microvascular networks will provide an enabling platform for a wide array of fluidic-based applications.

Three-dimensional (3D) microvascular networks with pervasive, interconnected channels less than 300 micrometres in diameter may find widespread application in microfluidic devices[1,2], including those used in biotechnology[3–6], autonomic materials[7], sensors[8], chemical reactors[9,10] and fluidic-based computers[11]. Although microchannel arrays are readily constructed in 2D by photolithographic[12] or soft-lithographic techniques[13], their construction in 3D remains a challenging problem. Previous efforts[12–14] have only yielded nominally planar devices, that is, 3D structures comprised of a few layers from repetitive lithographic processing, in which each layer requires a separate mask or stamp. Yet the construction of true 3D microvascular networks would open up new avenues for device design that would simultaneously allow for increased performance with a minimal planar footprint. Here, we demonstrate an easy approach for creating fluidic devices based on a 3D microvascular network of cylindrical microchannels. Such channels were directly assembled by robotic deposition, and then patterned to yield vertically oriented, square-spiral mixing towers within the device. Owing to their complex architecture, these vertical towers give rise to dramatic improvements in fluid mixing relative to simple straight (1D) and square-wave (2D) channels.

Control over fluid flow and mixing is difficult in microfluidic devices, where laminar flow and diffusive mixing are dominant[15]. The Reynolds number ($Re = Ul/\nu$, where U is the average flow speed, l is the characteristic cross-sectional dimension of the channel, and ν is the kinematic viscosity of the fluid) is the dimensionless ratio of inertial to viscous forces. Re is usually less than 100 under normal flow conditions[14] for microchannels of diameter (l) ~100 μm, a value far below that required (~2,500) for turbulent flow. Diffusive mixing is also slow relative to convection of the fluid in such channels, due to high values of the Péclet number[14] ($Pe = Ul/D_{mol} > 100$, where D_{mol} is the molecular diffusivity), which is the dimensionless ratio of convective to diffusive rates. This is of particular concern for mixing fluids that contain biological (for example, DNA or proteins) or other large molecules, because these species diffuse slowly[16]. As a result, prohibitively long path lengths are often required to ensure complete mixing in

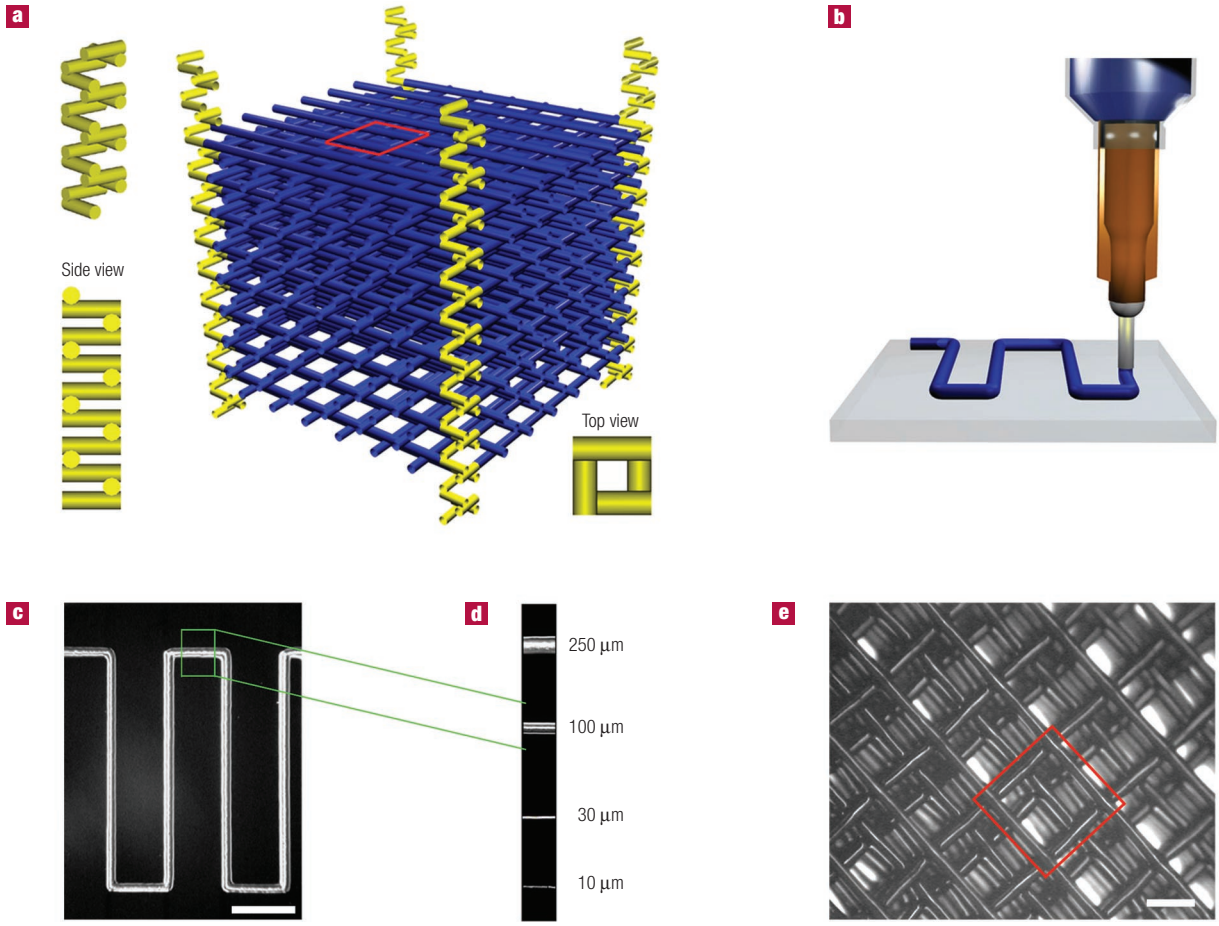

Figure 1 Microvascular scaffold fabrication. a, Square-spiral tower structure (yellow) embedded within the 3D microvascular network (blue). The red square denotes the top view shown in **e**. **b**, Robotic deposition of the fugitive organic ink (blue) through a cylindrical nozzle onto a moving *x*–*y* stage. **c**, Optical image (top view) of a 2D patterned feature within the microvascular scaffold. Scale bar = 1.0 mm. **d**, Ink filaments produced from different nozzle diameters (10–250 μm). **e**, Optical image (top view) of microvascular (16-layer) scaffold. Scale bar = 0.50 mm.

microfluidic devices. To reduce the planar footprint of such devices, recent efforts have focused on new design strategies for fluid mixing based on chaotic advection[12,14].

Chaotic advection promotes the rapid (exponential) stretching and folding of fluid interfaces within a complicated flow domain[17] that arises either through unsteadiness in the flow, or geometric complexity within the device. By exploiting this phenomenon at the microscale, the interfacial surface area across which diffusion may occur is greatly increased[17]. Two strategies have recently been advanced to promote chaotic advection of fluids within microchannels; one based on a 'twisted pipe' architecture[12] and the other involving bas-relief structures imprinted along the channel floor[14]. Although both strategies lead to enhanced mixing, device complexity remains limited due to the planar nature of the microscale fabrication methods used and the rectangular features obtained.

Directed assembly techniques such as robotic deposition[18–20], fused deposition[21–23], and two-photon polymerization[24,25] enable the easy construction of complex 3D structures at length scales (~300 μm or below) typically associated with microfluidic applications. To demonstrate the power of direct-write assembly, we have fabricated 3D microvascular networks based on the square-spiral architecture recently proposed by Toader and John[26]. Our assembly route consists of three key steps: (1) scaffold fabrication by robotic deposition of a fugitive organic ink; (2) scaffold infiltration with an epoxy resin followed by curing and fugitive ink extraction; and (3) subsequent infiltration of a photocurable resin followed by masking and photopolymerization to yield internally patterned features.

Sixteen-layer scaffolds were produced by robotic deposition of a paraffin-based organic ink in a layerwise build sequence (see Fig. 1). This direct-write technique uses an ink-delivery system mounted on a *z*-axis motion-control stage for agile printing onto a moving *x*–*y* stage. Ink was deposited through a cylindrical nozzle (diameter, $D = 200\ \mu m$) at the volumetric flow rate ($= 0.25\pi D^2 V$) required to maintain a constant deposition speed (V) of 15 mm s^{-1}. The viscoelastic properties of the ink were tailored to simultaneously permit flow during deposition while facilitating shape retention of the as-deposited filament, even as it spans gaps in the underlying layer(s). A 2D pattern of parallel cylindrical rods was created with an inter-rod separation distance of 1.25 mm. After a given layer was generated, the stage was incremented in the z direction ($\Delta z = 170\ \mu m = 0.85D$) and another layer was deposited with a 90° rotation and 0.5 mm planar shift from the underlying layer. This process was repeated until the desired 3D (16-layer) scaffold had been created.

Three-dimensional microvascular networks were fabricated by first infiltrating the 16-layer scaffold with an epoxy resin that cures under ambient conditions (see Fig. 2). Next, the fugitive scaffold structure was

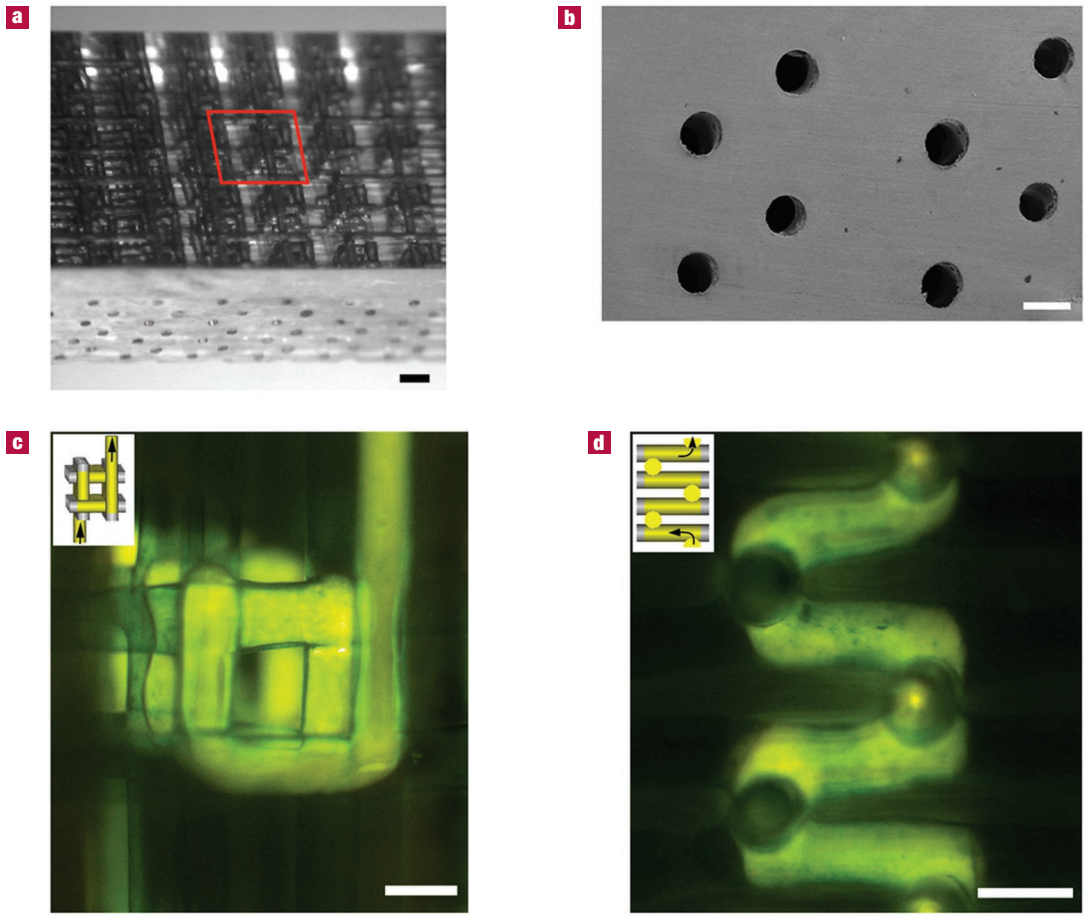

Figure 2 3D microvascular network fabrication. a, Optical image of 3D microvascular network embedded in clear epoxy matrix. Scale bar = 0.50 mm. The red square denotes the view shown in Fig. 1e. **b**, Scanning electron microscope image of the cross-section of this network. Scale bar = 250 μm. **c**, **d**, Fluorescent microscope images (**c**, top view; **d**, side view) of fluid (green) flowing inside a single tower structure illustrating its isolated nature. Scale bars = 250 μm. The corresponding schematic illustrations are located in the upper left corner of the two images where grey channels represent microchannels sealed by photopolymerization, yellow channels represent open microchannels, and the arrows indicate the direction of fluid motion. The cross-sectional views of the microchannels in the tower are occasionally obscured by stagnant fluid (within the channels) in the foreground such that the fluorescing flow stream is concealed in these regions.

removed by heating the material to 60 °C under a light vacuum leaving behind the microchannel array shown in Fig. 2b. Smooth, hydrophilic microchannels were produced with a root-mean-square (r.m.s.) surface roughness of 13.3 ± 6.5 nm.

Square-spiral mixing towers were isolated within the 3D microvascular networks by first infiltrating the microchannels with a photocurable resin followed by subsequent patterning and ultraviolet exposure (see Fig. 3). We adopted a flexible, inexpensive procedure for this latter step, which involved using a patterned transparency as a photomask coupled with a fluorescent microscope for alignment and exposure. Horizontal and vertical structures were isolated by rotating the specimen by 90° during the exposure process. On photopolymerization, the microchannels were immediately drained under vacuum and flushed with water to remove any unreacted resin. A 3D view of the final device reveals sealed and open microchannels that form the square-spiral mixing towers (see Fig. 3d). Two-dimensional slices taken through this device illustrate three distinct features, the epoxy matrix (light grey), microchannels sealed with photopolymerized resin (dark grey), and open microchannels (white). This simple approach is amenable to patterning a wide variety of regular geometries (for example, trigonal towers), however, more sophisticated routes such as two-photon polymerization by confocal microscopy would be required to produce 3D structures with arbitrary connectivity.

The mixing efficiency of the 3D square-spiral towers (Fig. 4c) was characterized by monitoring the mixing of two fluid streams (red and green) using fluorescent microscopy as a function of varying $Re \approx 0.15$–70. Fluid mixing was also characterized in two alternate microfluidic devices: a straight (1D) microchannel and a square-wave (2D) microchannel as shown in Fig. 4a,b, respectively. After the two fluid streams come into contact, the red and green fluorescent dyes begin to diffuse resulting in the formation of a yellow (mixed) fluid layer. Mixing occurs solely by molecular diffusion in the 1D device, which serves as a benchmark for evaluating mixing efficiency of both the 2D and 3D devices.

Optical images of the 1D, 2D and 3D microfluidic devices at representative low ($Re < 1$), intermediate ($1 < Re < 10$), and high Re (>10), are shown in Fig. 5a–c. A thin zone of mixed (yellow) fluid was observed at the centre of the 1D channel, whose width decreased with increasing Re due to a corresponding decrease in residence time at higher flow rates. At low and intermediate Re, a central zone of mixing appeared in the 2D device that followed the contour of the square channel array. At high Re, the mixing zone appears to undulate from the

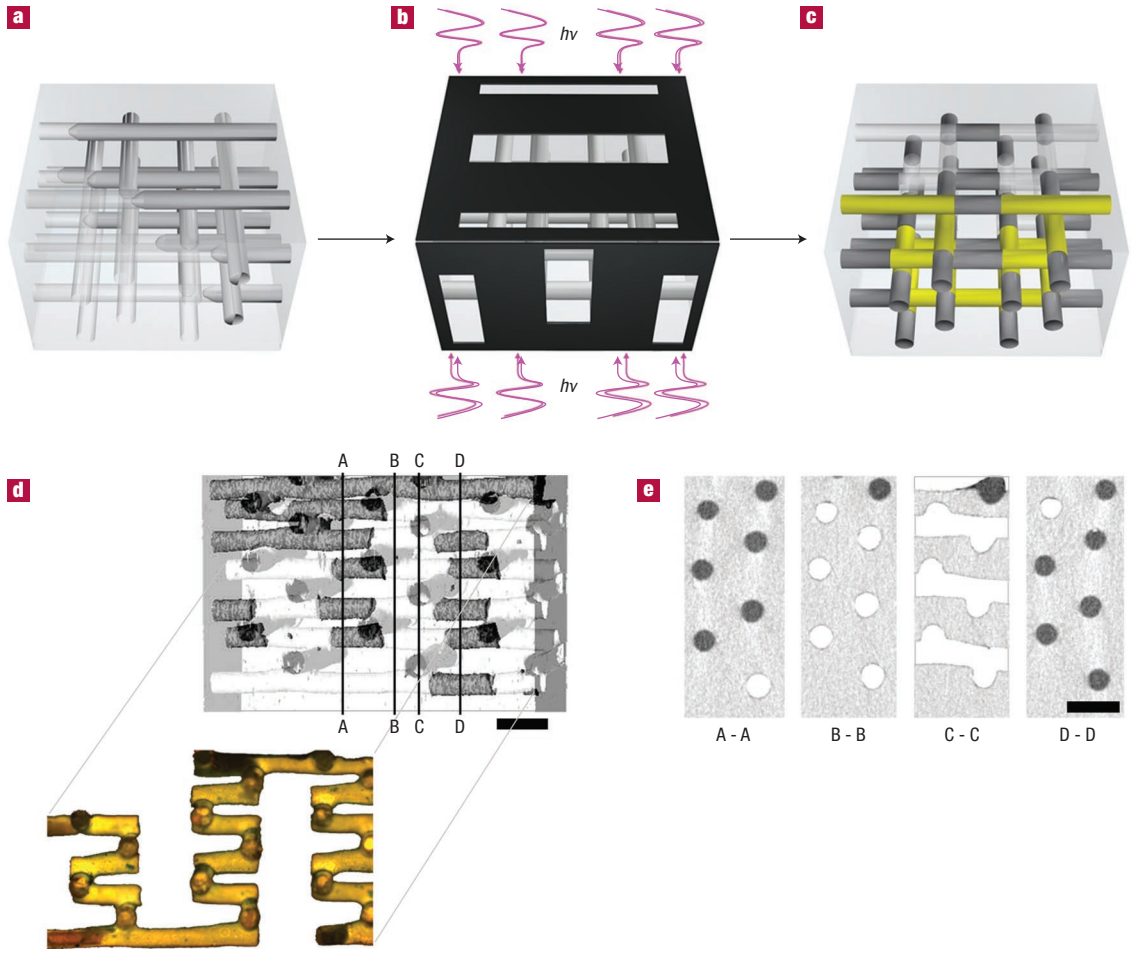

Figure 3 Square-spiral tower patterning. a–c, Schematic representation of photopolymerization procedure: **a**, infiltration of photocurable resin (dark grey) in the epoxy matrix (light grey); **b**, ultraviolet light ($h\nu$) exposure through photomasks (black); **c**, removal of unreacted resin. The polymerized regions are shown in darkest grey and the resulting tower structure is highlighted in yellow. **d**, Front perspective view of a 3D device acquired using X-ray tomography, showing sealed (dark grey) and open (white and light grey) microchannels after this procedure. The corresponding fluorescent microscope image of the infiltrated microchannel network is shown in overlay. Scale bar = 0.5 mm. **e**, Cross-sectional images of the network showing the sealed (dark grey) and open (white) microchannels at the bottom input (A–A), middle (B–B), edge (C–C), and the top output (D–D) of a square-spiral tower. Scale bar = 0.5 mm.

channel walls as fluid traverses through the array, at times filling the entire channel cross-section. The appearance of multiple mixing zones across the channel cross-section is indicative of transverse flow that twists and folds the fluid interface. In the 3D device, this behaviour was apparent even at low *Re* because the fluid stream is constantly reoriented by passing from segment to segment (90° turns) within the square-spiral towers. At intermediate *Re* the filtered image reveals increasing complexity in the flow domain with the appearance of multiple mixing zones and striations across the channel cross-section. At large *Re* the mixing process occurred rapidly and a fully mixed stream was achieved shortly after entering the second spiral tower.

To quantify the degree of mixing, the average yellow intensity $\langle I \rangle$ was measured across the channel and compared to the intensity obtained when the two fluids were completely mixed $\langle I_{mix} \rangle$ before their introduction to the channel. The relative intensity $\bar{I} = \langle I \rangle / \langle I_{mix} \rangle$ where $\langle\ \rangle$ denotes the average taken over all pixels imaged in a given microchannel segment, ranges from 0 (unmixed) to 1 (fully mixed). $\bar{I}$ is plotted as a function of streamwise distance in Fig. 5d for each microfluidic device at representative low and high *Re*. Diffusive mixing was the dominant mechanism observed for the 1D straight channel at all *Re* considered, as well as the 2D square-wave channel in the Stokes flow regime ($Re < 1$). The growth of the mixed zone normal to the flow direction (that is, the radial dispersion) scaled as $(D_{mol}t)^{1/2}$ (where $D_{mol} = 1.67 \times 10^{-6}$ cm^2 s^{-1}, and t is time), or as $x^{1/2}$ for steady flow conditions where x is the streamwise distance[27]. Mixing was markedly improved relative to diffusion alone for both the 2D square wave channel at high *Re* and in the 3D square-spiral towers over all *Re* studied. The oscillatory nature of the $\bar{I}$ data reflects the folding and twisting of the fluid interface as it is advected along a given channel within such structures. On viewing the 2D device from above, it seems that the mixed interface undulates across the channel when the streamlines periodically act to spin the interface into planar profile. In the Stokes flow regime, these oscillations are greatly exaggerated for the 3D device owing to the higher degree of twisting and folding of the mixing interface as the fluid stream negotiates each 90° turn within the tower. At higher *Re*, these oscillations are damped and complete mixing occurs rather quickly, within about 45 ms (or a streamwise distance of 6 mm) at $Re \sim 30$.

The relative intensity $\bar{I}$ is plotted as a function of *Re* in Fig. 5e for each microfluidic device. These data are reported at a constant streamwise distance of 14 mm, which corresponds to the outlet of the second tower

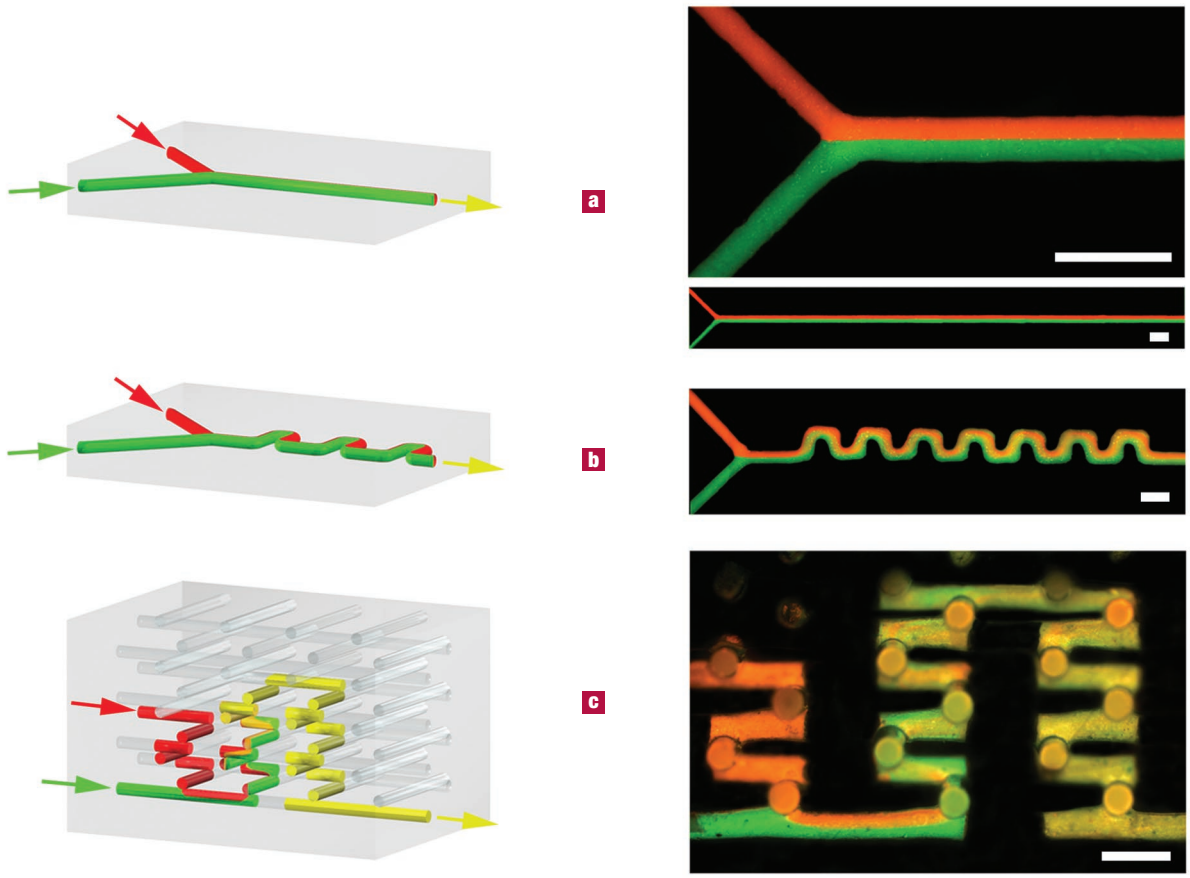

Figure 4 Microfluidic mixing experiments. a–c, Schematic representations and fluorescent microscope images of the 1D, 2D, and 3D microfluidic device mixing experiments, where two fluids (red and green) are mixed at $Re = 30.6$ to produce the yellow (mixed) output. The arrows indicate the flow direction. The two fluids meet at a Y-junction where they enter **a**, a 17-mm straight microchannel, and **b**, 15-mm (streamwise) square-wave microchannel with a series of seven C-turns. **c**, The two fluids are injected at discrete points within a 3D spiral tower before mixing within a series of two interconnected towers. All scale bars = 0.5 mm.

of the 3D device. The degree of mixing arising solely from diffusion under pure laminar flow conditions (1D case) decreased rapidly with increasing *Re*, as the residence time was reduced within the channel. Mixing in the 2D device was diffusion dominated at low *Re* before increasing linearly (see Fig. 5e) above $Re \approx 10$. Complete mixing was not observed for the 2D device until $Re \approx 70$. The mixing performance for the 3D microfluidic device was characterized by two distinct regimes. At low *Re*, diffusive mixing dominated, leading to a decrease in relative intensity as *Re* increased from 0.15 to ~1.0. It should be noted that this tower geometry led to a two-fold enhancement of mixing at $Re = 0.15$ relative to either the 1D or 2D case under the same conditions. At $Re \approx 1$, a transition in behaviour was observed and mixing was thereafter increasingly dominated by chaotic advection. Above this transition, mixing was greatly accelerated and nearly complete mixing was achieved at $Re > 15$. Although complete mixing remained diffusion-limited (that is, occurring over the diffusive length scale[27] $l_D = (D_{mol}t)^{1/2}$), chaotic advection stretched and folded the fluid interface into long tendrils and the flow domain consisted of interwoven striations of the two fluids. The separation distance between the striations for a steady, chaotically advecting flow, such as this one, will decrease exponentially with streamwise distance along the tower (compare $l_{sep} \approx 2A/l_0 \exp(\lambda t)$ for the time-dependent case, where A is the area of the flow domain, l_0 is the initial perimeter of the mixing two-fluid interface, and λ is the Lyapunov exponent of the advecting flow[27]). A homogenous mixture is obtained when the striation separations and the diffusion length are comparable. The relative intensity approached unity (fully mixed) at an exponential rate for the 3D square-spiral towers above this transition (see Fig. 5e), because the time scale for homogenization grows with natural log of the Péclet number[27] (that is, $t_{hom} \propto \ln(Pe)$). Such observations are taken as strong evidence for the dominance of chaotic advection in this regime.

The construction of 3D microvascular networks enables microfluidic devices with unparalleled geometric complexity. Such devices generate complicated flow patterns and enhanced fluid mixing over the entire range of *Re* investigated. The twofold increase in relative intensity observed for the vertical tower architecture at $Re < 1$ is significant, because the inertial forces (secondary flows) that induce stirring are exceedingly small in this regime. It suggests that geometrically complex architectures can have important ramifications on fluid flow over a broader range of conditions than previously considered. We anticipate that such effects may be further amplified using an alternate 3D microvascular network design that creates more complicated flow patterns within the device. At higher *Re*, the vertical towers served as highly efficient chaotic mixers. By fabricating networks comprised of

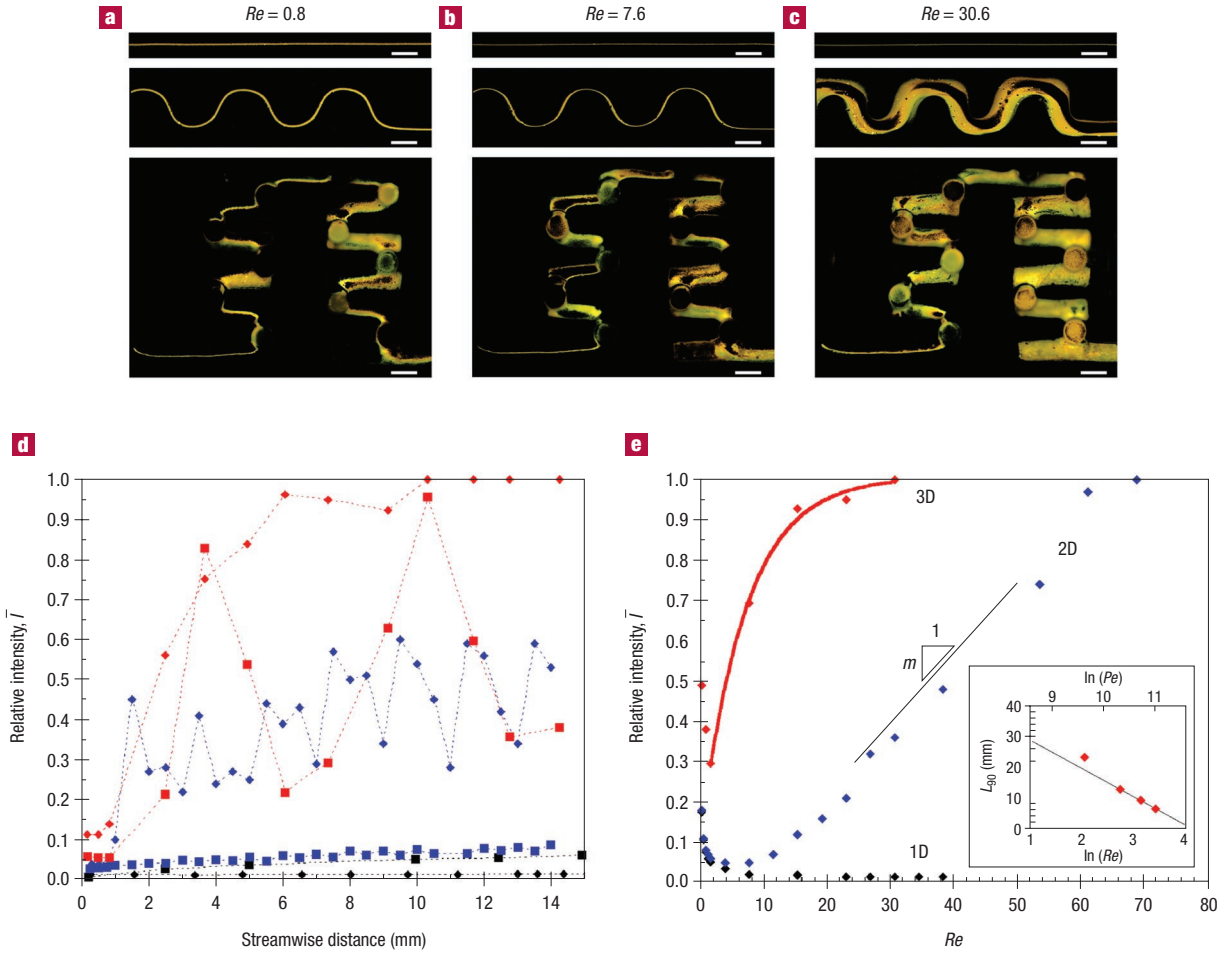

Figure 5 Microfluidic mixing results. a–c, Colour-filtered microscope images show the yellow mixed zone inside the 1D (top, streamwise distance shown = 13–16 mm), 2D (middle, streamwise distance shown = 10–16 mm), and 3D (bottom, streamwise distance shown = 0–14 mm) microfluidic devices at low, intermediate, and high flow rates (*Re*). All scale bars = 250 μm. **d**, Development of mixing with streamwise distance for the 1D (black), 2D (blue), and 3D (red) devices at low and high Reynolds numbers (squares, *Re* = 0.8; diamonds, *Re* = 30.6). **e**, Degree of mixing at the output (streamwise distance = 14 mm) for the 1D, 2D, and 3D microfluidic devices at different Reynolds numbers. Mixing within the 3D device exhibits an exponential dependence on *Re*, where $\bar{I} = 1 - \exp(-\beta \cdot Re)$ and $\beta = 0.354$ above $Re \approx 1$. Mixing within the 2D device shows a linear dependence $\bar{I} \propto mRe$ with $m = 0.0162$ above $Re \approx 10$. The length of channel (L_{90}) required to achieve 90% mixing ($\bar{I} = 0.9$) is plotted versus natural logarithm of *Re* (and the Péclet number, *Pe*) in the inset.

tens of layers, one can produce mixing elements whose planar footprint is defined solely by the cross-sectional area of a single tower. Compact fluidic factories for biotechnology, chemical reactor and fluidic-based computing applications could then be built by combining these individual elements in the form of integrated tower arrays.

Our approach opens up new avenues for device design that are inaccessible by conventional lithographic methods. Using our technique, which is amenable to many thermosetting polymers, one can rapidly transition from computer-aided design to 3D structures of varying architecture. Although we have demonstrated the benefits of using 3D microvascular networks as a basis for fluidic devices, it is envisioned that such networks could be applied more broadly. For example, combined with self-healing functionality[7], a 3D microvascular network provides an analog to the human circulatory system for the next generation of autonomic healing materials. The embedded network would serve as a circulatory system for the continuous transport of repair chemicals to the site of damage within the material. Thus, 3D microvascular networks furnish an enabling platform for a wide array of potential technological applications beyond fluidic mixing.

METHODS

MICROVASCULAR SCAFFOLD FABRICATION

Three-dimensional microvascular scaffolds were fabricated using a robotic deposition apparatus (Model JL2000, Robocasting Enterprises, Albuquerque, New Mexico). Three-axis motion was independently controlled by a custom-designed, computer-aided direct-write program (RoboCAD 2.0) that allowed for the construction of 3D structures in a layerwise deposition scheme. An organic ink (Prussian blue paste, Loctite, Rocky Hill, Connecticut) was housed in a syringe (barrel diameter = 4.6 mm, EFD, East Province, Rhode Island) and deposited onto a porous Teflon substrate (Airtech Performance Products, Huntington Beach, California). The total build time for the 16-layer scaffold was ~180 s.

MICROVASCULAR NETWORK FABRICATION

The microvascular scaffold was placed in a petri dish and cooled on a dry ice and acetone bath (–70 °C) before infiltrating the network with a liquid resin consisting of 2.5:1 epoxide (EPON 828, Shell Chemicals, Houston, Texas) to aliphatic amine curing agent (EPI-CURE 3274, Shell Chemicals). The porous substrate allowed entrapped air to escape during infiltration. The resin was cured at 22 °C for 24 h and then at 60 °C for 2 h. At 60 °C, the scaffold liquefied and could be removed under a light vacuum yielding the desired microvascular network of interconnected cylindrical microchannels. Their root-mean-square (r.m.s.) surface roughness, reported as an average of four scans taken at different streamwise distance within the microchannels, was measured with a Dektak 3030 profilometer (Veeco Instruments, Woodbury, New York).

3D MICROFLUIDIC DEVICE FABRICATION

A photopolymerizable resin (Model 61, Norland Products, Cranebury, New Jersey) was infiltrated into the microchannels comprising the microvascular network. This structure was then masked and selective channels were polymerized by ultraviolet flood exposure for 60 s. The photomask was generated by printing the desired pattern on a transparency using a high-resolution printer (5,080 d.p.i.). A filtered 100 W

ultraviolet light source (U-MNUA, type BP360-370, 360 nm wavelength) was mounted on an Olympus (Melville, New York) Epi-fluorescent microscope (BX-60) with a ×2 objective. 3D imaging of these devices was obtained by X-ray tomography on a Skyscan 1072 high-resolution desktop micro-CT system (Skyscan, Aartselaar, Belgium).

1D AND 2D MICROFLUIDIC DEVICE FABRICATION

The straight channel (1D) and square-wave channel (2D) microfluidic devices were fabricated by robotic deposition of an optically clear lubricant (CIP Lube, McGlaughlin Oil, Columbus, Ohio) onto a glass cover slide. The ink was housed in a syringe (barrel diameter = 4.6 mm, EFD) and deposited through a cylindrical nozzle (diameter, $D = 150\,\mu m$) at a constant deposition speed (V) of 6 mm s^{-1}. The 1D and 2D devices consisted of a single layer pattern of a 45° Y-junction connected to a 17-mm-long straight channel or a 15-mm-long square-wave channel with seven C-turns (size ~0.5 mm), respectively. The total build time was ~60 s for each patterned feature. Three rubber tubes were then placed at the two inlet and one outlet nodes associated with each patterned device. The tubes were filled with the deposition ink to ensure their connections to the deposited pattern. The patterned networks were encapsulated with the epoxy resin (2.5:1 epoxide to aliphatic amine curing agent) and cured at 22 °C for 24 h and 60 °C for 2 h. At 60 °C the organic ink was removed from the devices under a light vacuum. The surface roughness of microchannels in the 1D and 2D devices was also measured and found to be 14.4 ± 6.7 nm.

MIXING EXPERIMENTS

Mixing experiments were carried out in the 1D, 2D and 3D microfluidic devices by simultaneously flowing two aqueous fluids containing red or green fluorescent dyes (0.60 mg ml^{-1} of water, Bright Dyes, Miamisburg, Ohio). Mixing efficiency was characterized by measuring the yellow colour intensity produced on fluid mixing using a fluorescence light microscope (Zeiss Axiovert 100, Carl Zeiss Microimaging, Thornwood, New York) with a ×2.5 objective. The images were captured through a triple excitation filter (360/480/560) attached to a colour CCD camera controlled with MCID software (MCID v.6, Imaging Research, St. Catherines, Ontario, Canada). The fluids were housed inside 10 cm^3 syringes mounted side-by-side on a syringe pump (PHD 2000, Harvard Apparatus, Holliston, Massachusetts). In the 3D device, they were attached to Microfil (World Precision Instruments, Sarasota, Florida) syringe tips previously inserted in the two inlet pore channels (diameter ~230 μm) and sealed. For the 1D and 2D devices, the syringes were directly connected to the microchannels by the tubing inserted before resin infiltration. For each mixing experiment, a device was placed on the specimen stage of the fluorescent microscope and the two inputs were connected to the syringes containing the red and green fluorescent fluids, and the output was linked to a waste reservoir. The syringe pump was set to the desired flow rate (0.1–45 ml h^{-1}) and the mixing behaviour was then observed. All fluorescent images were captured under steady-state conditions (>180 s). A separate set of reference images were also obtained by flowing a premixed (yellow) solution of the fluorescent dyes through the microfluidic devices. Image processing was performed with Photoshop (Photoshop v.6, Adobe, San Jose, California) for colour filtering and MCID (as before) for pixel intensity measurements. Intensity data were normalized by the reference intensities acquired at identical streamwise distances to account for small intensity variations due to adsorption or scattering in the epoxy structure (see Fig. 3d). All intensity measurements were taken in the horizontal channel sections of the spiral tower structures.

Received 4 October 2002; accepted 26 February 2003; published 23 March 2003.

References

1. Anderson, J. A. *et al.* Fabrication of topologically complex three-dimensional microfluidic systems in PDMS by rapid prototyping. *Anal. Chem.* **74,** 3158–3164 (2000).
2. Ikuta, K., Hirowatari, K. & Ogata, T. Three dimensional micro integrated fluid systems (MIFS) fabricated by stereo lithography. *Proc. IEEE MEMS 1994* 1–6 (1994).
3. Burns, M. A. *et al.* An integrated nanoliter DNA analysis device. *Science* **282,** 484–487 (1998).
4. Chou, H.-P., Spence, C., Scherer, A. & Quake, S. A microfabricated device for sizing and sorting DNA molecules. *Proc. Natl Acad. Sci.* **96,** 11–13 (1999).
5. Strömberg, A. *et al.* Microfluidic device for combinatorial fusion of liposomes and cells. *Anal. Chem.* **73,** 126–130 (2001).
6. Choi J.-W. & Ahn, C. H. An active microfluidic mixer for mixing of microparticles and liquids. *SPIE Proc.* **4177,** 154–161 (2000).
7. White, S. R. *et al.* Autonomic healing of polymer composites. *Nature* **409,** 794–797 (2001).
8. Chabinyc, M. L. *et al.* An integrated fluorescence detection system in poly(dimethylsiloxane) for microfluidic applications. *Anal. Chem.* **73,** 4491–4498 (2001).
9. Losey, M. W., Schmidt, M. A. & Jensen, K. F. Microfabricated multiphase packed-bed reactors: characterization of mass transfer and reactions. *Ind. Eng. Chem. Res.* **40,** 2555–2562 (2001).
10. Jeon, N. L. *et al.* Generation of solution and surface gradients using microfluidic systems. *Langmuir* **16,** 8311–8316 (2000).
11. Moore, S. K. Microfluidics for complex computation. *IEEE Spectrum* **38,** 28–29, (2001).
12. Liu, R. H. *et al.* Passive mixing in a three-dimensional serpentine microchannel. *J. Microelectromech. Syst.* **9,** 190–197 (2000).
13. McDonald, J. C. *et al.* Fabrication of microfluidic systems in poly(dimethylsiloxane). *Electrophoresis* **21,** 27–40 (2000).
14. Stroock, A. B. *et al.* Chaotic mixer for microchannels. *Science* **295,** 647–651 (2002).
15. Pfahler, J., Harley, J., Bau, H. & Zemel, J. Liquid transport in micron and submicron channels. *Sens. Actuat. A* **21-23,** 431–434 (1990).
16. Jendrejack, R. M., de Pablo, J. J. & Graham, M. D. Stochastic simulations of DNA in flow. Dynamics and the effects of hydrodynamic interactions. *J. Chem. Phys.* **116,** 7752–7759 (2002).
17. Aref, H. The development of chaotic advection. *Phys. Fluids* **14,** 1315–1325 (2002).
18. Chrisey, D. B. Materials processing: the power of direct writing. *Science* **289,** 879–881 (2000).
19. Cesarano, J. & Calvert, P. Freeforming objects with low-binder slurry. US Patent 6,027,326 (2000).
20. Smay, J. E., Cesarano, J. & Lewis, J. A. Colloidal inks for directed assembly of 3D periodic structures. *Langmuir* **18,** 5429–5437 (2002).
21. Zein, I., Hutmacher, D. W., Tan, K. C. & Teoh, S. H. Fused deposition modeling of novel scaffold architectures for tissue engineering applications. *Biomaterials* **23,** 1169–1185 (2002).
22. Too, M. H. *et al.* Investigation of 3D non-random porous structures by fused deposition modeling. *Int. J. Adv. Manuf. Technol.* **19,** 217–223 (2002).
23. Allahverdi, M., Danforth, S. C., Jafari, M. & Safari, A. Processing of advanced electroceramic components by fused deposition technique. *J. Euro. Cer. Soc.* **21,** 1485–1490 (2001).
24. Borisov, R. A. *et al.* Fabrication of three-dimensional periodic microstructures by means of two-photon polymerization. *App. Phys. B* **67,** 765–767 (1998).
25. Cumpston, B. H. *et al.* Two-photon polymerization initiators for three-dimensional optical data storage and microfabrication. *Nature* **398,** 51–54 (1999).
26. Toader, O. & John, S. Proposed square spiral microfabrication architecture for large three-dimensional photonic band gap crystals. *Science* **292,** 1133–1135 (2001).
27. Jones, S. W. in *Chaos Applied to Fluid Mixing* (eds Aref, H. & El Naschie, M. S) 185–196 (Pergamon, Oxford, 1995).

Acknowledgements

This work has been sponsored by the AFOSR Aerospace and Materials Science Directorate (Grant no. F49620-00-1-0094) and the National Science Foundation (Grant no. DMI 00-99360 and DMR-01-177792). Electron microscopy was carried out in the Center for Microanalysis of Materials, University of Illinois, which is supported by the US Department of Energy. Support for D. Therriault came from the University of Illinois through a CARVER Fellowship and a Nanoscience and Technology Center Fellowship, and the government of Québec (NATEQ). The robotic deposition apparatus used in this work was designed and built by J. Cesarano, and customized software for 3D fabrication was developed by J.E. Smay. The authors gratefully acknowledge the thoughtful comments and technical advice of colleagues R. Adrian, H. Aref, J. Moore, N. Sottos and P. Wiltzius.
Correspondence and requests for materials should be addressed to S.R.W. and J.A.L.

Competing financial interests

The authors declare that they have no competing financial interests.